In summary, this work demonstrates freestanding high-κ ferroelectric HZO membranes grown by pulsed laser deposition and transferred onto 2D semiconductors to enable high-performance MoS_2 FETs. Owing to strong ferroelectricity, a dielectric constant of ~20.6, and an excellent interface quality (Dit ≈ 9×10^{10} cm^{-2} eV^{-1}), the devices achieve Ion/Ioff ≈ 10^9 and a minimum subthreshold swing of 53 mV dec^{-1}. Integrated logic circuits and scalable short-channel operation highlight HZO membranes as a CMOS-compatible dielectric platform for advanced 2D and 3D integrated electronics. (Reported by Cheng-Maw Cheng)

This report features the work of Jan-Chi Yang, Yen-Fu Lin and their collaborators published in Nat. Electron. ***8****, 560 (2025).*

TPS 09A Temporally Coherent X-ray Diffraction
TPS 45A Submicron Soft X-ray Spectroscopy
TLS 13A1 X-ray Scattering

- Soft-X-ray absorption spectroscopy, X-ray diffraction
- Materials Science, Condensed-matter Physics

Reference

1. C.-Y. Lin, B.-C. Chen, Y.-C. Liu, S.-F. Kuo, H.-C. Tsai, Y.-M. Chang, C.-Y. Kuo, C.-F. Chang, J.-H. Chen, Y.-H. Chu, M. Yamamoto, C.-H. Shen, Y.-L. Chueh, P.-W. Chiu, Y.-C. Chen, J.-C. Yang, Y.-F. Lin, Nat. Electron. **8**, 560 (2025).

An "*s*-Electron" Donor Band Drives the Metallic Ferromagnetism in Co-Doped ZnO Films

Polarization-dependent, bulk-sensitive hard X-ray photoemission spectroscopy reveals that a metallic "s-electron" character donor band mediates ferromagnetism in Co-doped ZnO films and solves a long-standing problem in dilute magnetic materials.

Diluted magnetic semiconductors (DMSs) hold great potential for spintronic applications and continue to attract significant attention as room-temperature ferromagnetic (RTFM) materials. While doping transition metals (TMs) into oxide semiconductors is a common approach, the underlying physical mechanism remains poorly understood, particularly for the diluted magnetic oxide (DMO) Co-doped ZnO (Co:ZnO) films, which exhibit high Curie temperatures (T_C) exceeding 300 K. The most promising mechanism proposed for high-T_C ferromagnetism is the donor impurity band exchange model, in which donor electrons mediate the coupling between TM spins. However, the nature of the donor band electrons has not yet been identified experimentally. Based on a well-planned set of experiments, including material synthesis, magnetic measurements, X-ray absorption near-edge and extended X-ray absorption fine-structure spectroscopy (XANES, EXAFS), and polarization-dependent, bulk-sensitive hard X-ray photoemission spectroscopy (HAXPES), Jung-Chun-Andrew Huang (National Cheng Kung University) and his collaborators have now demonstrated that the donor band originates in $Zn^{1+}4s^1$ states in Co:ZnO epitaxial films.[1] The study provides new insight into the ferromagnetic mechanism in Co:ZnO, where $Zn^{1+}4s^1$ states mediate ferromagnetism, leading to Co^{2+} spin ordering and metallic-like transport. These results elucidate the complementary roles of dopant and host electronic states and open avenues for designing novel room-temperature DMSs.

It is well-known from the donor impurity band exchange mechanism proposed by Coey *et al.*[2] that hybridization between TM states and defects influences the magnetic and electrical properties of DMOs. In ZnO-based DMOs, impurity bands arising from defects or TM 3*d* states can behave as localized states at low density and retain semiconducting behavior, or they can broaden with increased defect density and exhibit metallic transport. Accordingly, the authors first developed fabrication methods that preserve structural defects in the films. Epitaxial Co-doped ZnO films were grown using radio-frequency magnetron sputtering (RF sputtering) on sapphire substrates, maintaining a low Co doping concentration (~5 at%) to avoid percolation effects. The films were carefully optimized to preserve structural defects, such as zinc interstitials and oxygen vacancies. For a comparative analysis, four sets of samples were prepared

on Al_2O_3 (0001) substrates by RF sputtering in this study. The concentration of oxygen vacancies was controlled by varying the H2 content mixed with Ar during deposition. Samples A and B contained 5 at% Co doping in a 40 nm Co:ZnO layer. The H_2/Ar ratios during sputtering were 5% for sample A and 2.5% for sample B. After deposition, both samples were capped with a 2 nm ZnO protective layer with no H_2 exposure during sputtering. Sample C was structurally identical to sample A but lacked the ZnO protective layer. These samples facilitate the investigation of the presence and absence of defects, such as oxygen vacancies, while eliminating charging effects during HAXPES measurements and thereby enable a reliable comparison of their relationship with variation in magnetic properties. In addition, to compare the effects of Co doping on ZnO, a highly conductive ZnO film (40 nm) was prepared, denoted as sample D, using a 2.5% H_2/Ar ratio during growth. The growth parameters of samples A, B, C, and D are summarized in **Table 1**.

Table 1: Growth parameters for samples A, B, C, and D.

	Capping Layer	Main Layer	H_2/Ar Ratio during Sputtering
Sample A	2 nm ZnO	40 nm Co (5 at%):ZnO	5%
Sample B	2 nm ZnO	40 nm Co (5 at%):ZnO	2.5%
Sample C	none	40 nm Co (5 at%):ZnO	5%
Sample D	none	40 nm ZnO	2.5%

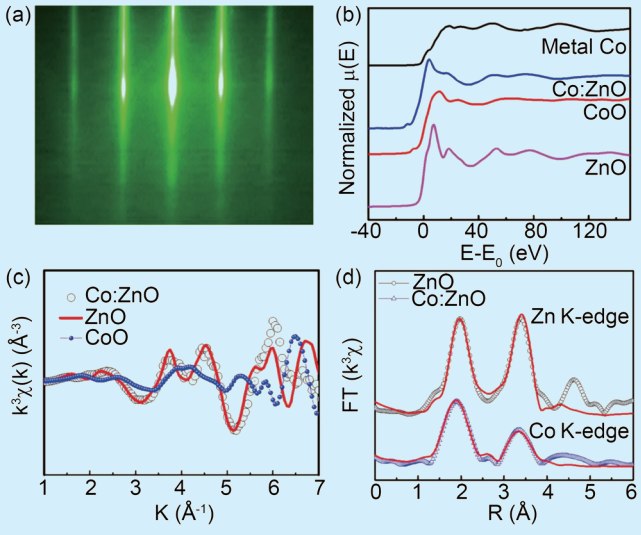

Fig. 1: (a) RHEED pattern of the $Co_{0.05}Zn_{0.95}O$ film along the [11-20] azimuth, indicating high crystallinity. (b) Normalized XANES spectra at the Zn K-edge for undoped ZnO (sample D) and at the Co K-edge for Co (5 at%)-doped ZnO (sample A), compared with reference spectra from CoO powder and Co metal foil. (c) k^3-weighted χ(k) functions at the Zn K-edge (ZnO) and Co K-edge (Co:ZnO), with CoO as reference. (d) Fourier transformed EXAFS spectra of Co:ZnO at the Co K-edge and ZnO at the Zn K-edge. The overlaid fitting curve for Co:ZnO shows a local structural environment closely resembling that of Zn in ZnO. [Reproduced from Ref. 1]

The epitaxial films were characterized by reflection high-energy electron diffraction (RHEED), as shown for one case in **Fig. 1(a)**. XANES experiments at Taiwan-contract beamline BL12B2 in SPring-8 [**SP 12B1**](**Fig. 1(b)**) were conducted to confirm that the Co atoms exhibit divalent Co^{2+} spectral features by comparison with a reference CoO sample. This was also confirmed by the HAXPES Co 2*p* spectrum and configuration interaction cluster model calculations. The authors then performed EXAFS measurements for the Co:ZnO samples, CoO, and ZnO. The data were analyzed using Fourier-transformed EXAFS spectra for all samples to demonstrate that the doped Co atoms occupy the Zn sites in the Co:ZnO epitaxial films, as shown in **Figs. 1(c) and 1(d)**.

Magnetization (M) versus magnetic field (H) measured at room temperature for H in the in-plane direction is shown in **Fig. 2**, confirming clear ferromagnetism in the Co:ZnO samples with a protective layer. The M–H hysteresis loops for samples A and B reveal saturation magnetization (M_S) values of approximately 1.09 and 0.38 μ_B/Co, respectively, as shown in **Fig. 2**. In contrast, the M_S values of sample C and sample D (ZnO) are very small, less than 0.05 μ_B/Co. These findings indicate the crucial role of both magnetic doping and structural defects in achieving RTFM in Co:ZnO. Furthermore, the magnetic properties of Co:ZnO without the protective layer (sample C) were monitored over time by exposing the samples to ambient conditions. The results indicated a monotonic decay in the ferromagnetic signal over time, reinforcing the critical role of both magnetic doping and structural defects in obtaining RTFM in Co:ZnO. Although similar findings have been reported in the literature, direct evidence for the presence of an impurity band in defect-protected Co:ZnO was not provided in earlier studies.

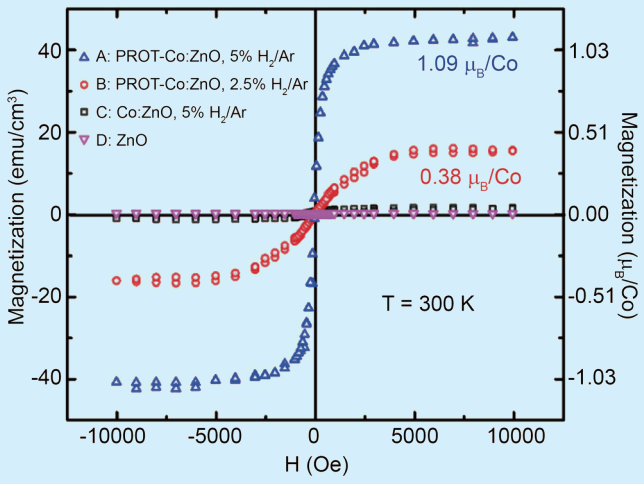

Fig. 2: Magnetization of samples A, B, C, and D at room temperature. The data have been corrected for the linear diamagnetic contribution of the sapphire substrates. [Reproduced from Ref. 1]

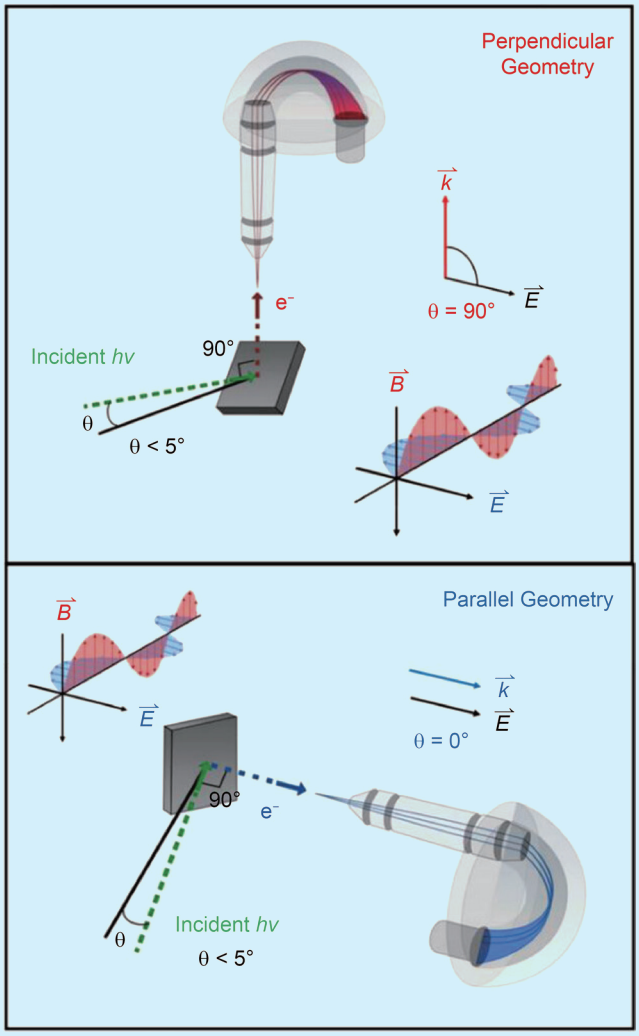

Fig. 3: Experimental geometry of the polarization dependent HAXPES setup is defined by the angle θ between the incident photon beam electric field vector $\vec{E}$ and the momentum $\vec{K}$ of photoemitted electrons. The incident photon beam is linearly polarized with the electric field vector within the horizontal plane of the synchrotron ring. Top: In the perpendicular polarized geometry (also called s-polarized, where s stands for senkrecht≡perpendicular, in German), we use a vertically mounted analyzer, θ = 90°, and then $\vec{K}$ is perpendicular to $\vec{E}$. Bottom: In the parallel geometry, also called the p-polarized geometry, we use a horizontally mounted analyzer, θ = 0°, and $\vec{K}$ is parallel to $\vec{E}$. Then, based on the angular dependence of differential ionization cross-sections, one can distinguish features due to s-, p-, d-,...type photoemitted electrons in a sample from the measured spectral intensities in the parallel and perpendicular geometries. [Reproduced from Ref. 1]

A key advantage of using HAXPES experiments with high incident photon energy is the enhanced probing depth, which enables the access to the intrinsic bulk electronic structure. Most importantly, polarization-dependent HAXPES can resolve the orbital character of electronic states in the valence band. Accordingly, polarization-dependent HAXPES measurements were performed at the Taiwan-contract beamline BL12XU in SPring-8, Japan [**SP 12U1**]. The experimental setup enables independent detection of photoelectrons with momentum components both perpendicular and parallel to the electric field of nearly grazing incidence (< 2°) synchrotron light, as schematically illustrated in **Fig. 3**.[3,4] The authors first conducted polarization-dependent HAXPES of the O 1*s*, Co 2*p*, and Zn 2*p* core levels of Co:ZnO samples. After normalizing the spectra to the Zn 2*p*3/2 core level main peaks, the results confirmed that the O 1*s* spectra, with a main peak at 530.36 eV and a weaker feature at 531.34 eV, showed clear polarization dependence with significantly higher intensity in the parallel geometry compared to the perpendicular geometry. In contrast, the Co 2*p* peaks did not show evidence of polarization dependence, while the results confirmed that the Co ions are divalent Co^{2+}.

Next, the authors measured the HAXPES data for the parallel and perpendicular geometries within 6 eV BE for samples A–D, as shown in **Figs. 4(a) and 4(b)** on the next page. The results revealed a band at approximately 2.7 eV but with significantly different spectral intensities. The spectral intensity of this feature showed the same trend in both geometries; it is maximum for sample A and decreases for sample B and gets further reduced for sample C, while the feature is totally missing in sample D, it follows the magnetization magnitude of the samples and indicates that the 2.7 eV BE feature is due to Co 3*d* states. Note that although sample B exhibited a lower defect concentration (H_2/Ar ratio of 2.5%), it was protected by a capping layer, whereas sample C, with a higher defect concentration (H_2/Ar ratio of 5%), remained uncapped. Since the long-range ordered high-T_C samples A and B are nearly metallic, the authors conducted a high signal-to-noise ratio examination of the HAXPES data at and near E_F to check for the donor band, as shown in **Figs. 4(c) and 4(d)**. For samples A–C shown in **Fig. 4(c)**, the data reveal a band peaked at around 0.3 eV below E_F in samples A and B and crosses E_F with finite intensity; however, this feature is absent in sample C. More importantly, the 0.3 eV peak is strongly suppressed in the perpendicular geometry for samples A and B. It is important to note that the HAXPES signal associated with Zn 4*s* orbitals is reduced by the polarization factor in the perpendicular geometry. Thus, the magnitude of its spectral weight reduction, combined with the absence of the feature in sample C—which includes Co 3*d* states at 2.7 eV BE, as seen in **Figs. 4(a) and 4(b)**—indicates that the 0.3 eV feature originates from a predominantly Zn 4*s* character metallic donor band, as measured by HAXPES. Finally, to validate the Zn 4*s* character of the donor band, we measured the polarization dependence of sample D, as shown in **Fig. 4(d)**. The results reveal an electron donor band even for sample D. While it is weaker than the donor bands observed in samples A and B, it shows qualitatively similar polarization dependence, with strongly suppressed spectral intensity in the perpendicular geometry, akin to the electron donor bands seen in Co-doped ferromagnetic samples A and B. Since sample D does not contain Co 3*d*

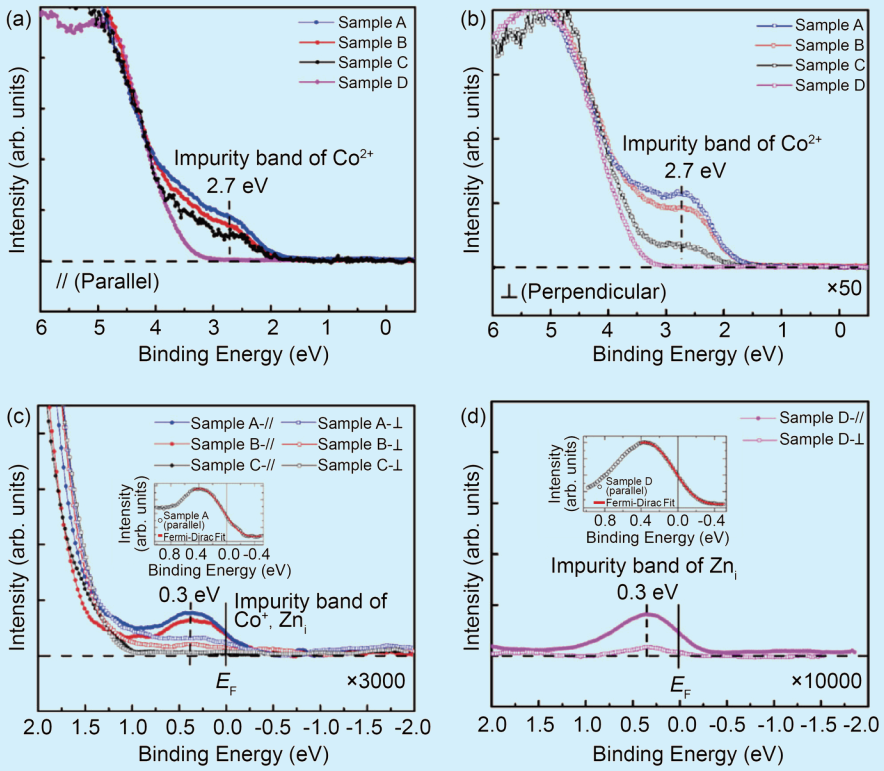

Fig. 4: (a) Valence band HAXPES spectrum measured in parallel geometry, serving as the reference for the y-axis scale across all panels in this figure. (b) Magnified view (×50) relative to the y-axis scale of (a), showing the valence band HAXPES spectrum acquired under the perpendicular geometry. (c) Highly magnified view (×3000) relative to the y-axis scale of (a), comparing the valence band HAXPES spectra of samples A, B, and C measured in the parallel and perpendicular geometries. Inset: Fermi edge observed in sample A in the parallel geometry. (d) Further magnified view (×10000) relative to the y-axis scale of (a), displaying the valence band HAXPES spectra of sample D in parallel and perpendicular geometries. Inset: Fermi edge observed in sample D in parallel geometry. [Reproduced from Ref. 1]

dopants, this result unambiguously indicates that the donor band originates from Zn 4*s* character electrons.

The authors conclude that polarization-dependent HAXPES measurements provide direct evidence of an impurity donor band in Co-doped ZnO, characterized by a Zn 4*s* metallic band crossing the Fermi level. This supports the Ruderman-Kittel-Kasuya-Yosida model for high-T_C ferromagnetism in Co-doped ZnO. This finding offers new insights into the ferromagnetic mechanism, wherein $Zn^{1+}4s^1$ states mediate ferromagnetism in Co-doped ZnO. (Reported by Ashish Chainani)

This report features the work of Jung-Chun-Andrew Huang and his collaborators published in Adv. Sci. ***12****, e08148 (2025).*

SP 12B1 Materials X-ray Study
SP 12U1 Hard X-ray Photoelectron Spectroscopy

- XANES, EXAFS, HAXPES
- Materials Science, Condensed-matter Physics

References

1. P.-Y. Chuang, J.-C. A. Huang, A. Chainani, H.-S. Hsu, Y.-F. Liao, C.-Y. Sung, C.-H. Liu, C.-Y. Liao, C.-H. Lee, K.-D. Tsuei, Adv. Sci. **12**, e08148 (2025).
2. J. M. D. Coey, M. Venkatesan, C. B. Fitzgerald, Nat. Mater. **4**, 173 (2005).
3. J. Weinen, A. Fiedler, M. Merkel, D. Flahaut, S. Cramm, B. Ruck, J. Electron Spectrosc. Relat. Phenom. **198**, 6 (2015).
4. F. Offi, G. Panaccione, A. Fondacaro, P. Torelli, N. B. Brookes, G. Rossi, Nucl. Instrum. Methods Phys. Res. A **550**, 454 (2005).